Indian Journal of Pure & Applied Physics
Vol. 59, November 2021, pp. 756-767

Unsteady Casson Fluid Flow Subject to Natural Convection and Quadratic Free Convection along with Applied Transverse Magnetic Field

R Balamurugan & A Vanav Kumar*

Mathematics Division, Department of Basic and Applied Science, National Institute of Technology, Arunachal Pradesh, Jote Campus, Papum Pare District, Arunachal Pradesh-791 113, India

Received 26 October 2020; accepted 7 October 2021

In the present study, Casson fluid flow past an instantly stretched sheet is studied. The initial fluid flow is of Crane type. At $t' \geq 0$, the fluid is subject to sudden stretching as well as Quadratic free convection along with the application of a sudden transverse Magnetic field. This sets in unsteadiness in the fluid flow. As time progresses, $t' \to \infty$, the fluid flow becomes steady. The fluid flow settles down to steadiness at different time intervals for different values of parameters. The parameters include Quadratic free convective parameter, Grashof number, transverse magnetic field parameter, and Casson fluid parameter. The numerical computations are carried out using the well-established Crank-Nicolson method. Validation of numerical computations is carried out by comparing the results of computations with analytic solutions at a steady state for applicable cases. Our results are in good agreement with the analytic solutions. Plots for Horizontal velocity, Vertical velocity, Temperature field, local Skin friction, and local Nusselt number are described. Transient progressive profiles of the dependent variables are described to understand the nature of unsteadiness. The results show that the Quadratic free convection can be utilized to control the fluid flow to obtain finer results.

Keywords: Casson fluid, Crane type, Crank-Nicolson method, Magnetic field, Quadratic free convection

1 Introduction

Fluid past a stretching sheet has attracted the interest of many researchers, industrial investigators due to its applications in industries like glass manufacturing, plastic industry, textile industry, dye-making industry, metal sheet, manufacturing industry, *etc*. In this regard, with such a large scale of industries, naturally, they require theoretically available solutions both in the form of closed-form analytical as well numerical solutions. They also require small-scale experimental results performed at research labs to implement the solutions in their manufacturing units. In this regard and significance concerning the present report, Crane[1] solutions are treated as parent investigation, which provides closed-form solutions for momentum equation and energy equation for the fluid flow past a stretching plate. The utilization of solutions provided by Crane[1] paved the way to obtain the closed/analytic form solutions of fluid flow with heat and mass transfer with suction/blowing over a stretching sheet and was published by Gupta & Gupta[2]. Closed-form solutions were obtained for magnetohydrodynamic fluid past a permeable stretching sheet by Kumaran *et al*.[3]. In their investigation, the stretching sheet was considered to be quadratic, with linear suction or blowing. Plots described the streamline distribution across the domain. The finite difference method applied to moving surfaces was also considered by various investigators. Ganesan & Palani[4] have used the implicit finite difference method for solving the transient free convective problem. In their problem, they consider the magnetohydrodynamic fluid flow with variable heat and mass flux. The flux is power law in nature. Prasad[5] employs the finite difference method which solves the unsteady fluid flow problem with radiation and mass transfer effects included in them. The transient effect is set in the two-dimensional flow due to suddenly moving infinite vertical plate. The scheme is an implicit finite difference method of the Crank-Nicolson type. Muthucumaraswamy & Ganesan[6] solve transient system which involves heat gradient and mass transfer. The study reports the transient effects, which are set in due to impulsively started vertical plate, maintained at rest initially. Investigation using the finite difference method can be found in Arifuzzaman *et al*.[7], Mondal *et al*.[8] & Rabbi *et al*.[9]. report the non-

*Corresponding author: (Email: vanavkumar.a@gmail.com)

Newtonian, convective transient boundary layer flow of viscoelastic nanofluids with thermal radiation along with a vertical (semi-infinite) porous plate with periodic magnetohydrodynamics. They report their results through streamlines and isotherms after validating the results in the literature. Mondal *et al.*[8] use the explicit finite difference method to investigate the transient changes in the Casson fluid. The fluid is subject to changes in patterns in time due to the effect of the sudden application of a movement of the plate along the direction of flow. The fluid is also subject to the impact of fickle viscosity and thermal conductivity along with suction. The method used is the explicit finite difference technique and results compared with the literature for simplified cases. They report the effects on the dependent variable velocities, temperature field, concentration, local skin friction τ_X, local Nusselt number, Nu_X and local Sherwood number, Sh_X. Rabbi *et al.*[9] also published research related to explicit finite difference technique and Casson fluid flow. The study reports the results of Casson fluid parameter, thermo diffusion coefficient, Eckert number, Brownian diffusion coefficient, Chemical reaction parameter, Magnetic parameter, Lewis number, Permeability parameter, *etc* on the dependent variables and their derivatives. Bêg *et al.*[10] report the non-isothermal, nonlinear magneto convection effect on the boundary layer free convective flow of fluid with heat and mass transfer. The flow is physically subject to ion slip currents, joule heating, viscous heating, and Hall current. The study uses the Keller box scheme method to extract the solutions. Apart from an investigation involving finite difference techniques, the present investigations address the nature of the flow of Casson fluid.

Casson fluid has attracted a lot of investigators in the recent past and will continue to do so in the future. Ramesh & Devakar[11] provide the analytical solution for fluid flow of Casson type. They consider the flow with slip boundary conditions. The nature of the fluid is Couette flow. Solutions in closed form were also provided by Kataria & Patel[12]. They provide the solution for Casson fluid subject to magnetic force. The fluid is subject to thermal diffusion, heat generation/radiation, and chemical reaction. In their study, the vertical plate which is embedded through a porous medium is subject to oscillation resulting in unsteadiness. Khan *et al.*[13] study the effect of shear stress on the fluid of Casson type. The fluid flow passes through the vertical plate. They provide analytical solutions when the stress is of step function and oscillatory concerning time. Casson fluid flow past a non-linearly stretching sheet was investigated by Ahmed *et al.*[14]. The fluid is subject to slip conditions. The stretching sheet is nonlinear (that is, power-law in nature concerning the distance from the origin). The study involves addressing the Entropy generation. Khan *et al.*[15] consider the Casson fluid reacting chemically. Mahanthesh & Greesha[16] study the dusty Casson fluid flow. They study the Thermal Marangoni convection in two-phase flow. Fluid and dust particle temperature is a quadratic function of interface arc length. The ordinary differential equations thus obtained are evaluated using the Runge-Kutta-Fehlberg method. Patel[17] addresses the issue of Casson fluid flow subject to cross-diffusion and heat generation on mixed convection. The fluid is also subject to flow through a porous medium, transverse magnetic field, and non-linear thermal radiation. The fluid flow is subject to a porous medium. Raza[18] reports the convective stretching sheet with slip and thermal radiation of Casson fluid flow near the stagnation point. The partial differential equations (PDEs) are transformed to ordinary differential equations (ODEs) using similarity transformation. The obtained ODE's are then solved using Runge-Kutta-Fehlberg (RKF) method. A comparative study of Maxwell and Casson fluid was carried out by Kumar *et al.*[31]. They adopt the Buongiorno[19] model for governing equations. Casson fluid flow has been subject to the wavy surface too by Prasad *et al.*[20]. Their investigation report the mixed convection, double-diffusive in the presence of Darcian porous medium. Mackolil & Mahanthesh[21] report the statistical solutions along with the exact solutions for Casson fluid flow past a vertical plate. The flow is unsteady subject to radiation and the Dufour effect. Abdelmalek *et al.*[22] report the effect of activation energy on the Casson fluid flow. The magnetohydrodynamic Casson fluid flow is subject to Stefan blowing effects and the results are addressed in their investigation.

Recently, there is an interest among researchers to investigate the effect of Quadratic free convection on the fluid flow past moving surfaces. Quadratic free convection or non-linear natural convection was used by Venkatadri *et al.*[29]. They carried out their study to understand the flow patterns inside a square cavity which is driven by the lid. The nature of micropolar

fluid flow was reported by Reddy *et al*.[30]. Quadratic free convection is included in the fluid flow through an inclined flat plate which has the effect in a non-Darcy porous medium. Their study includes a variety of densities concerning changes in temperature and concentration. Dusty Casson and dusty Carreau fluid flow's nature including the quadratic natural convection was investigated by Mahanthesh *et al*.[16]. Heat source/sink effects which are non-uniform are included in their investigation of fluid flow. Balamurugan & Kumar[28] have recently carried out the study on Casson fluid flow including the quadratic natural convection past a stretching sheet where the initial flow of the fluid is non-zero.

Apart from the above studies, continuous investigations are carried. Selvaraj *et al.*[32] explore the solutions which are obtained through the analytic method for parabolic stream and its rotation effect near a impenetrable viscous and electrically coordinating fluid past a reliable quickened unbound isothermal perpendicular plate in the proximity warmth and mass trade in the presence of MHD. Rabbi *et al.*[33] has researched the effects of MHD, radiation (thermal), and chemical reaction on Casson Nanofluid past a stretching sheet. They implement their solutions through the explicit finite difference method. Krishna *et al*.[34] studies the effects on MHD convective flow which pasts through an infinite absorbent vertical plate. Kumar *et al.*[35] investigate the results through the efficient Galerkin method of Radiation, Soret, and Dufour, Hall current effects over an infinite vertical plate fixed in a porous media. Narahari *et al.*[36] implement the Crank-Nicolson finite difference method to the transient natural convective two-dimensional boundary layer nanofluid past a vertical plate with constant heat flux with the additional effect of Brownian motion and thermophoresis. Correlation results of local (state) Nusselt number for the limiting case are being performed in their analysis. Implementation of the Crank-Nicolson method was also carried out by Umamaheswar *et al.*[37] who studied the unsteady non-Newtonian viscoelastic second-order Rivlin-Erickson MHD fluid in the presence of thermal radiation, thermal diffusion, viscous dissipation, radiation absorption, heat absorption, and homogeneous chemical reaction with constant mass flux. Prasad *et al.* studied the free convection for the MHD steady fluid flow with heat and mass transfer in a non-Darcy porous medium along with the Soret and Dufour effects. They implement the Keller-Box implicit finite difference scheme to evaluate the partial differential equations. Syafiqah & Narahari[39] carry out the studies of amplified velocity effects on the unsteady natural convective fluid past a plate with nanoparticle migration and heat transfer behavior subject to heat flux. They adopt the second-order accurate Crank-Nicolson finite difference method to extract the solutions of the transformed governing equations. Adaptation of the same scheme is also done by Narahari *et al*.[40] to solve the non-homogeneous convective nanofluid flow past a moving unsteady vertical plate. Astuti *et al.*[41] study the nanofluid's natural convection past a vertical plate which is set to acceleration with variable wall temperature depending on time. They employ the Crank-Nicolson method to solve the partial differential equation in two independent variables.

There occurs problems in the industry where the fluid flow is uniform. Fluid flow at a specific instant is subject to introduction to physical interference. This may be in the form of the introduction of dye(s) in the textile industry, molding of metal sheets with the introduction of magnetic fields, changing the temperature of the fluid, *etc*. All this physical change results in a significant change in the end product whether in the form of garments, metal plates, or plastic molds. All these products have one thing in common, the introduction of physical effects at a specific time instance in an already set uniform motion.

In the present investigation, it is this part the authors wish to report. In the problem, the fluid flow which is assumed to be viscous fluid (Casson fluid), initially is flowing with a predefined velocity. At a certain instant of time, the fluid is subject to physical changes. This introduction of physical changes disturbs the flow behavior from steady to unsteadiness. The unsteadiness so generated then settles down to an adapted steady flow.

As the authors believe the behavior of fluid flow due to these effects is an important topic to be addressed, the present investigation has been carried out.

In the next section, the concept is modeled through mathematical equations namely the governing equations. Then the mathematical governing equations are simplified to non-dimensional forms. Section 3 reports the method by which the numerical computation is carried out. Section 4 describes the

plots and includes illustrations to understand the plots and hence the fluid behavior. The paper ends with a conclusions section about the present study and prospects.

2 Problem Formulation

Consider an incompressible laminar unsteady Cassonfluid flowing past a stretching sheet. The Casson fluid initially flows with the horizontal velocity, u', vertical velocity, v' respectively. The horizontal and vertical directions are given by x' and y'-axis. The magnitude of the velocities initially, $(t'<0)$, is given by $u'=c'x'\exp\left(-\sqrt{\frac{c'}{\upsilon}}y'\right)$ and $v'=-\sqrt{c'\upsilon}\left(1-\exp\left(-\sqrt{\frac{c'}{\upsilon}}y'\right)\right)$, respectively, which are nothing but the closed-form solutions obtained by Crane[1]. Here t', c', υ are the time, stretching parameter (>1), and kinematic viscosity of the fluid. The stretching sheet issues through the coordinate axis at $y'=0$, along with the mentioned conditions and the fluid being subject to wall temperature given by

$$T'-T'_\infty=\left(T'_w-T'_\infty\right)\frac{\exp\left(-\sqrt{\frac{c'}{\upsilon}}\right)F\left(\Pr,\Pr+1,-\Pr\exp\left(-\sqrt{\frac{c'}{\upsilon}}y'\right)\right)}{F\left(\Pr,\Pr+1,-\Pr\right)}$$

where T', T'_∞, T'_w, $\Pr$ are the transient temperature, the temperature at far of a distance from the sheet, temperature at the wall, and Prandtl number. The expression $F(.)$ is the hypergeometric function. At $t'\geq 0$, the sheet is stretched with a velocity proportional to the distance from the origin given by $c'x'$, where c' is the proportionality constant (stretching constant, (>1)), with wall temperature changing to $T'-T'_\infty=T'_w-T'_\infty$. The fluid is subject to quadratic free convection along with free convection and applied transverse magnetic field. For an incompressible and isotropic flow, the rheological equation of the state of a Casson fluid is given by Kataria[13],

$$\tau_{ij}=\begin{cases}2\left(\mu_B+\dfrac{P_y}{\sqrt{2\prod_c}}\right)E_{ij}, & \prod>\prod_c\\ 2\left(\mu_B+\dfrac{P_y}{\sqrt{2\prod_c}}\right)E_{ij} & \prod<\prod_c\end{cases}, \qquad \ldots (1)$$

where τ_{ij} is the $(i,j)-$th component of the stress tensor, μ_B is the plastic dynamic viscosity of the non-Newtonian fluid, and P_y is the yield stress of the fluid. The product of the component of deformation rate with itself is given The letter $\prod$ gives its product of the component of deformation rate. E_{ij} are the (i,j)-th component of the deformation rate, and as earlier mentioned the relation connecting the two is given by the expression $\prod=E_{ij}E_{ij}$. The critical value , $\prod_c$, is this product is based on the non-Newtonian fluid. So, Solid type or motion type behavior is observed if the shear stress is less than the applied yield stress to the fluid or if the shear stress is greater than the yield stress.

Assuming negligible Reynold's magnetic number, invoking the Boussinesq's approximation, the model for the fluid flow obeying the above conditions are given by the governing equations,

$$\frac{\partial u'}{\partial x'}+\frac{\partial v'}{\partial y'}=0, \qquad \ldots (2)$$

$$\frac{\partial u'}{\partial t'}+u'\frac{\partial u'}{\partial x'}+v'\frac{\partial u'}{\partial y'}=\upsilon\left(1+\frac{1}{\gamma}\right)\frac{\partial^2 u'}{\partial y'^2}+\rho g\beta\left(T'-T'_\infty\right)+\rho g\beta^*\left(T'-T'_\infty\right)^2-\frac{\sigma B_0^2}{\rho}u', \qquad \ldots(3)$$

$$\frac{\partial T'}{\partial t'}+u'\frac{\partial T'}{\partial x'}+v'\frac{\partial T'}{\partial y'}=\frac{\kappa}{\rho C_p}\frac{\partial^2 T'}{\partial y'^2}, \qquad \ldots (4)$$

$$t'<0,\quad \forall \quad x',y'>0:$$

$$u'=c'x'\exp\left(-\sqrt{\frac{c'}{\upsilon}}y'\right), \qquad \ldots (5)$$

$$v'=-\sqrt{c'\upsilon}\left(1-\exp\left(-\sqrt{\frac{c'}{\upsilon}}y'\right)\right), \qquad \ldots (6)$$

$$\frac{T'-T'_\infty}{T'_w-T'_\infty}=\frac{e^{-\sqrt{\frac{c'}{\upsilon}}y'}F\left(Pr,Pr+1,-Pre^{-\sqrt{\frac{c'}{\upsilon}}y'}\right)}{F\left(Pr,Pr+1,-Pr\right)} \qquad \ldots (7)$$

$$t' \geq 0, \quad y' = 0:$$
$$u' = c'x', \qquad \ldots (8)$$

$$v' = 0, \qquad \ldots (9)$$

$$T' - T'_{\infty} = T'_{w} - T'_{\infty}, \qquad \ldots (10)$$

Applying the dimensionless variables $t = t'c'$, $x = x'\sqrt{\frac{c'}{\upsilon}}$, $y = y'\sqrt{\frac{c'}{\upsilon}}$, $u = \frac{u'}{\sqrt{c'\upsilon}}$, $v = \frac{v'}{\sqrt{c'\upsilon}}$, $T = \frac{T' - T'_{\infty}}{T'_{w} - T'_{\infty}}$, $\gamma = \mu_B \sqrt{2\prod_c} / P_y$, $Gr = \frac{\rho g \beta \left(T'_w - T'_\infty\right)}{c'\sqrt{c'\upsilon}}$, $Gr^* = Gr\beta^* \left(T'_w - T'_\infty\right)$ and $\Pr = \frac{\kappa}{\mu C_P}$ non-dimensionalizing (1)-(3) along with the initial conditions and boundary conditions (4)-(5), we get,

$$\frac{\partial u}{\partial x} + \frac{\partial v}{\partial y} = 0, \qquad \ldots (11)$$

$$\frac{\partial u}{\partial t} + u\frac{\partial u}{\partial x} + v\frac{\partial u}{\partial y} = \left(1 + \frac{1}{\gamma}\right)\frac{\partial^2 u}{\partial y^2} + GrT + Gr^* T^2 - Mu', \qquad \ldots (12)$$

$$\frac{\partial T}{\partial t} + u\frac{\partial T}{\partial x} + v\frac{\partial T}{\partial x} = \frac{1}{\Pr}\frac{\partial^2 T}{\partial y^2}, \qquad \ldots (13)$$

$$t < 0, \quad \forall \quad x, y > 0:$$
$$u = x\exp\left(-y\right), \qquad \ldots (14)$$

$$v = -\left(1 - \exp\left(-y\right)\right), \qquad \ldots (15)$$

$$T = \frac{e^{-y} F\left(Pr, Pr+1, -Pre^{-y}\right)}{F\left(Pr, Pr+1, -Pr\right)}, \qquad \ldots (16)$$

$$t \geq 0, \quad y = 0:$$
$$u = x, \qquad \ldots (17)$$

$$v = 0, \qquad \ldots (18)$$

$$T = 1, \qquad \ldots (19)$$

where, Gr, Gr^* are the Grashof number, and Quadratic free convection parameter.

3 Computational method for the Mathematical model

The non-dimensional equations Eqs. (11-13) along with non-dimensional initial and boundary conditions (14) to (19) are solved using the implicit finite difference method of Crank- Nicolson type[5,6]. The forward difference for first-order derivative terms concerning time, the backward difference for first-order derivative terms along the horizontal direction, the central difference for the second-order derivative terms along the vertical direction are applied for discretization. The method is unconditionally stable[29, 30]. The computation is carried out for the domain $0 \leq x \leq 1$ and $0 \leq y \leq 15$ with the mesh size kept at $x = 0.002$, $y = 0.01$, and $t = 0.001$ along the x, y-axis, and time, t respectively.

Numerical experiments were performed to take care that the profiles for all the discussed cases did not change significantly or encounter any abrupt changes. Considering these numerical experiments the domain was so chosen such that the profiles are captured smoothly and that there is no variation in the final values (steady-state) of the dependent variable to a certain tolerance limit. The stopping criteria of the iterations are set less than or equal to 5×10^{-5} for the dependent variables namely, the dimensionless horizontal velocity and the dimensionless temperature profile, u, T.

In check that the given scheme is in order, the error computations were made for $Gr = Gr^* = 0.0$. For this case the Eqs. (11) and (12) admit closed-form solutions. Consequently, the exact local skin friction is given by $-\tau_x = \frac{\partial u}{\partial y} = x\sqrt{1+M}$ (Kumaran *et al.*[23]) The Fig. 1(a,b) shows the comparison of exact and computed local skin friction profile. One can observe from the profile that the profiles of computed as well as the exact values are in agreement for the two magnetic parameter numbers ($M = 0.0$ and 12.0).

This shows that our computations are in order and hence, we can proceed to extract results of importance.

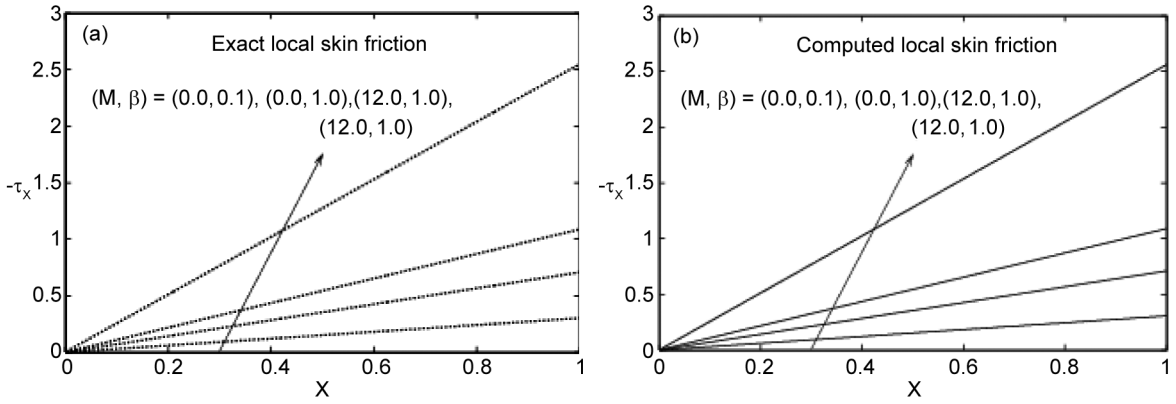

Fig. 1(a) — Exact local skin friction, Kumaran *et al.*[23] and (b) Computed local skin friction.

Therefore, it becomes opt for carrying out computations further for non-zero values of Grashof number and Quadratic free convection parameter, *Gr* and *Gr** respectively. Consequently, we discuss the results in the following section.

The dimensionless local Nusselt number is given by [24],

$$Nu_X = -x \left.\frac{\partial T}{\partial y}\right|_{y=0} .$$

4 Results and Discussion

The results in Fig. 2-16 and Fig. 21-22, are described for $\beta = 0.1$ and Fig. 17-19 for $\beta = 1.0$.

Fig. 2 describes the horizontal velocity of the fluid flow due to the increasing value of the strength of the magnetic field, *M*. The *M* value increases from 0.0 to *12.0* as shown in the plot. This is a fact in the literature. This slowdown or decrease in the horizontal velocity is due to Lorentz's force which arises due to the application or introduction of an applied magnetic field. The Lorentz force can hold down/suppress the flow of fluid[12]. In this figure the plots are made for the Quadratic convection parameter, *Gr**, being zero that is there is no free nonlinear natural convection. Also, the Grash of number, *Gr*, is zero indicating that there is no natural convection. The plots in the figure, hence, are free from any natural convection effects and indicate the behavior of the fluid due to the applied magnetic field alone. The steady-state curves (or plots) described here have encountered a non-zero velocity of the fluid at the time, *t = 0*. Hence, they are of significance and different from the study on MHD literature. Earlier study analog to the present study was carried out by cited literature[23-28]. It must be noted that these plots

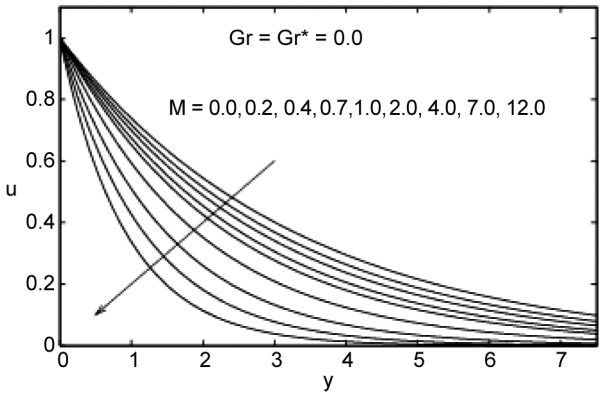

Fig. 2 — Steady-state horizontal velocity profiles, $\beta = 0.1$

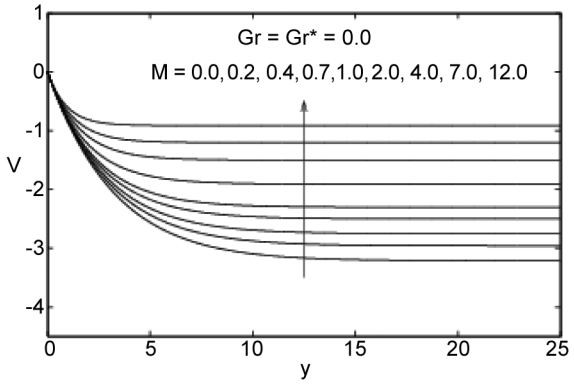

Fig. 3 — Steady-state vertical velocity profiles, $\beta = 0.1$

are again the once same as Kumaran *et al.*[23] for *M = 0, 1.0*. One can observe that there is a sharp change in the slope of the curves as the magnetic force gets increased.

Figure 3. represents the steady vertical velocities of the fluid in absence of natural convection and Quadratic natural convection. Again, the profiles are under the influence of the magnetic field alone. These contours are extracted using the continuity equations,

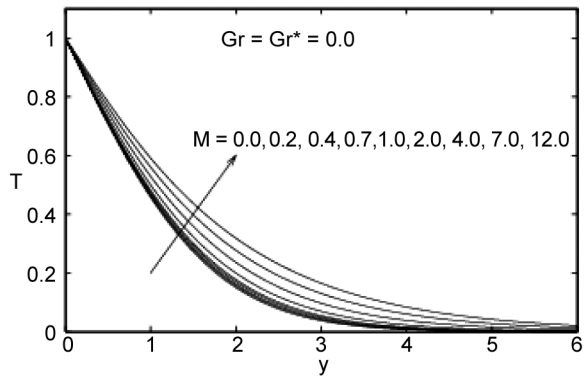

Fig. 4 — Steady-state temperature profiles, $\beta = 0.1$

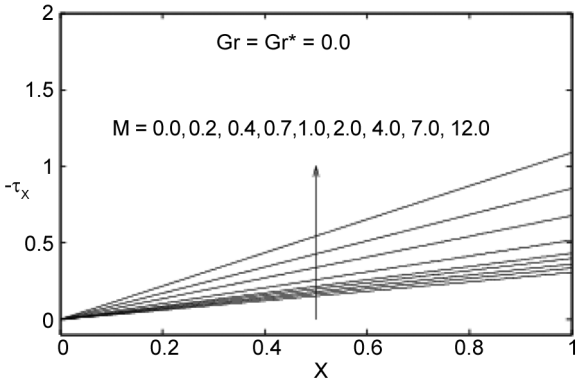

Fig. 5 — Steady local skin friction, $\beta = 0.1$

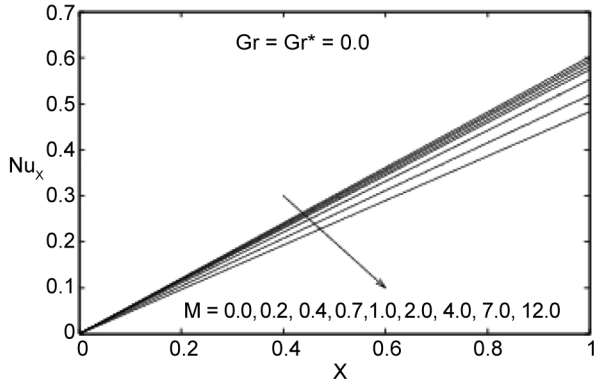

Fig. 6 — Steady Nusselt number, $\beta = 0.1$

since, the fluid flow must satisfy the law of conservation of mass. They are opposite in sign and the vertical velocity flux across the vertical axis is opposite to horizontal velocity flux across the horizontal axis. Fig. 4. represents the temperature field, which shows an increase as the power of the applied transverse magnetic field increases. The temperature change is proportional to the values of the magnetic parameter. For *M = 0.0, 0.2, 0.4, 0.7, 1.0*

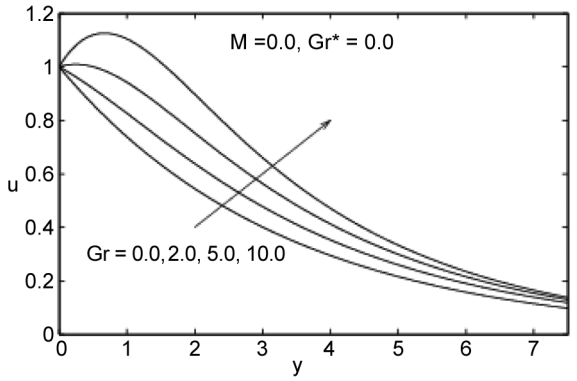

Fig. 7 — Steady-state horizontal velocity profiles, $\beta = 0.1$

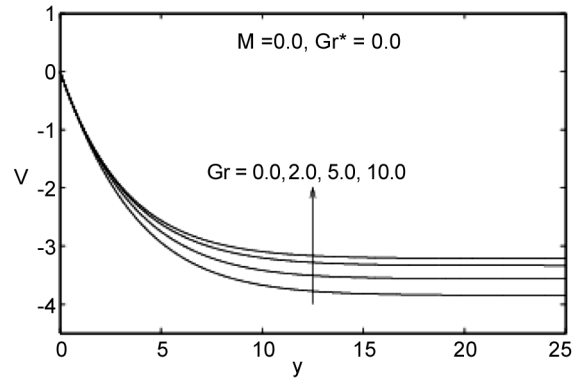

Fig. 8 — Steady-state vertical velocity profiles, $\beta = 0.1$

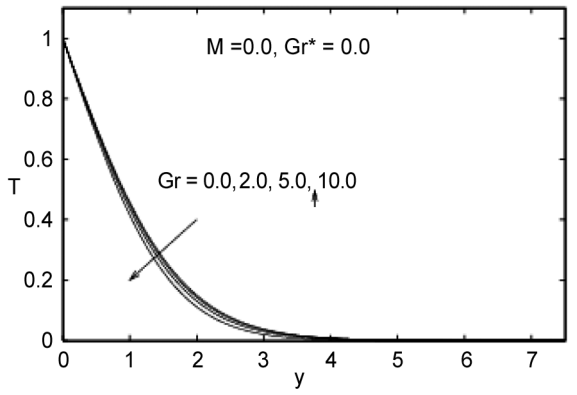

Fig. 9 — Steady-state temperature profiles, $\beta = 0.1$

the profiles are clustered together compared to the profiles of temperature for *M = 2.0, 4.0, 7.0, 12.0*. They are more distinct and separate from each other as the magnetic parameter increases.

Similarly, Fig. 5-6, represents the effect of applied transverse magnetic effect on local skin friction and local Nusselt numbers. One can conclude the facts observing the plots and they are consistent with

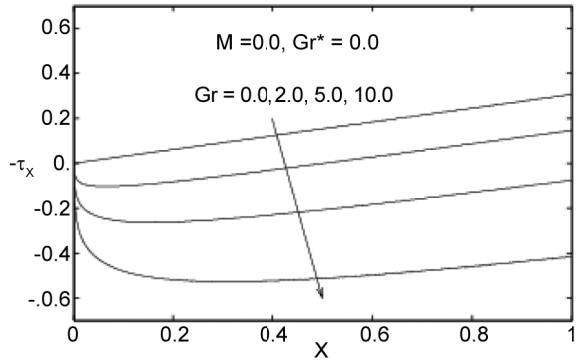

Fig. 10 — Steady local skin friction, $\beta = 0.1$

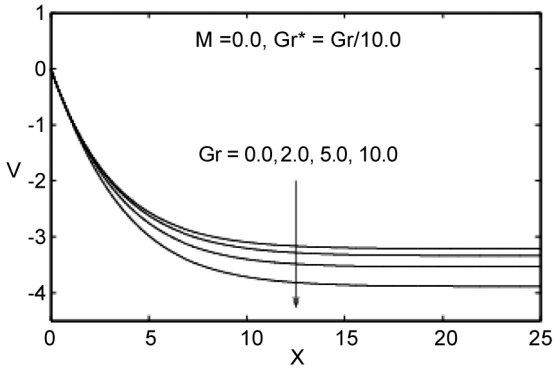

Fig. 13 — Steady-state vertical velocity profiles, $\beta = 0.1$

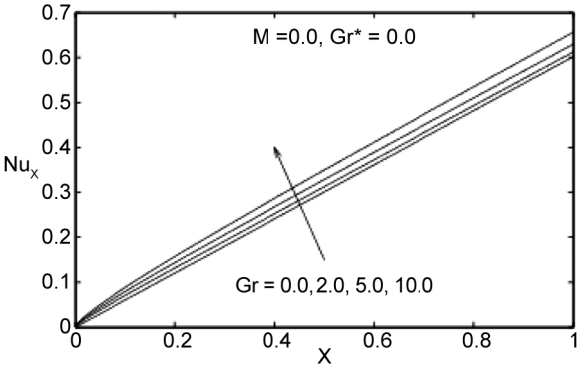

Fig. 11 — Steady Nusselt number, $\beta = 0.1$

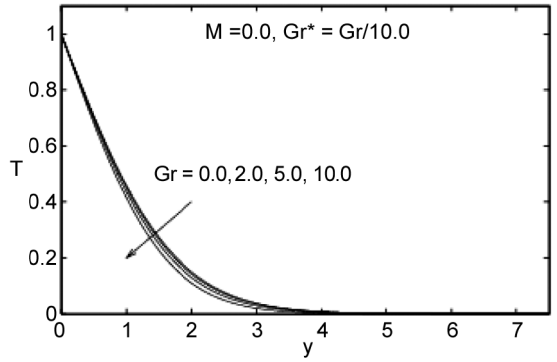

Fig. 14 — Steady-state temperature profiles, $\beta = 0.1$

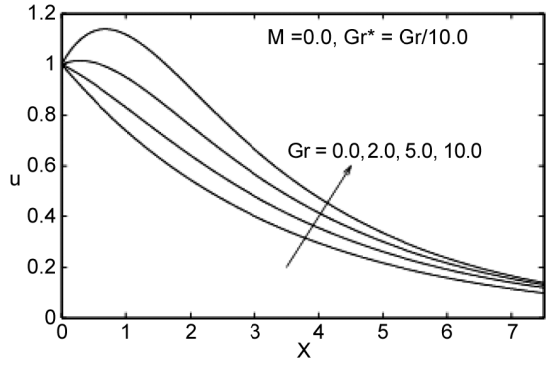

Fig. 12 — Steady-state horizontal velocity profiles, $\beta = 0.1$

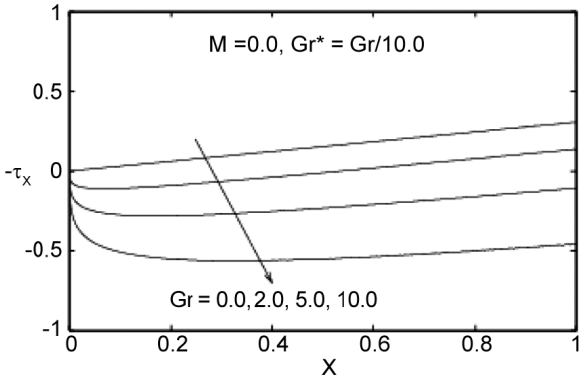

Fig. 15 — Steady local skin friction, $\beta = 0.1$

results available in the literature. The local skin friction increases significantly concerning applied magnetic strength. This is logical since the applied magnetic strength suppresses the fluid flow thereby increasing the friction. The fluid flow tends to get slowed down, which is being reflected in the plot, Fig. 5. The local Nusselt number behavior is similar to the local skin friction, except that the applied magnetic field has an opposite effect on the local Nusselt number. Here, the heat transfer rate increases as the magnetic strength increase as observed in the plots, Fig. 6.

Fig. 7-11 represents the velocity/local skin friction (τ_x)/local Nusselt number(Nu_X) profiles for Grashof number, *Gr = 0.0, 2.0, 5.0,* and *10.0*. The horizontal/vertical velocity increases with an increase in the natural convection. Again the Nusselt number profiles cannot be distinguished for the values of $M \leq 1.0$ compared to values $M > 1.0$.

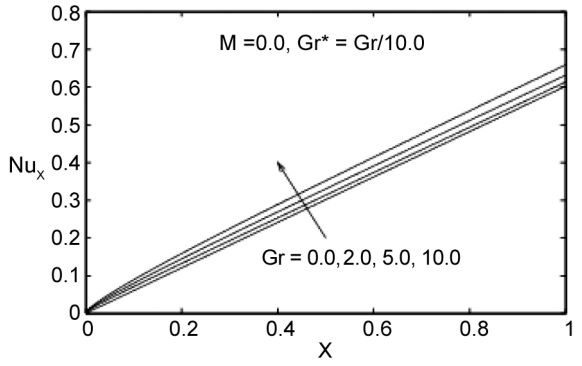

Fig. 16 — Steady Nusseltnumber, $\beta = 0.1$.

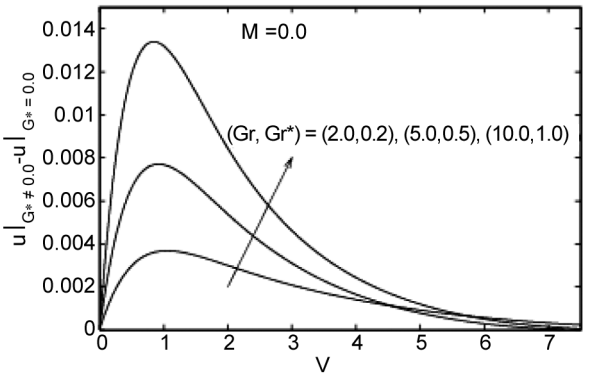

Fig. 17 — Difference between the horizontal profiles, $\beta = 1.0$.

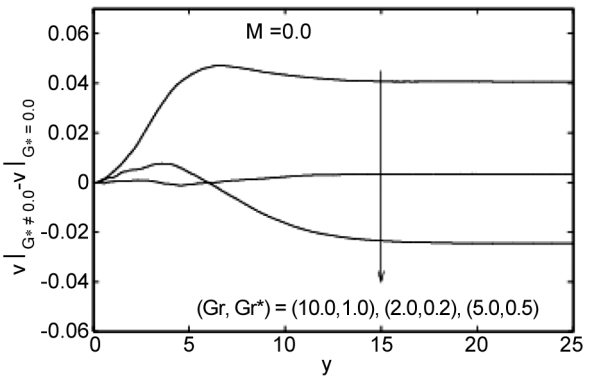

Fig. 18 — Difference between the vertical velocity profiles, $\beta = 1.0$.

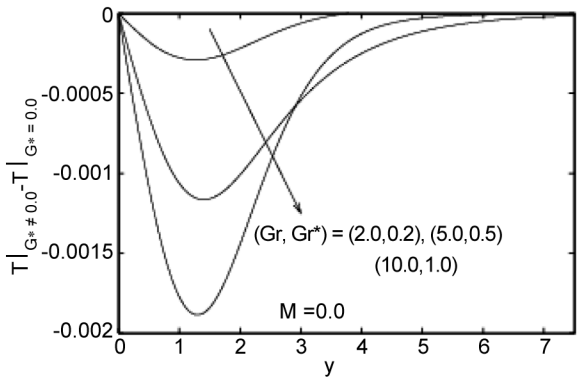

Fig. 19 — Difference between the Temperature profiles, $\beta = 1.0$.

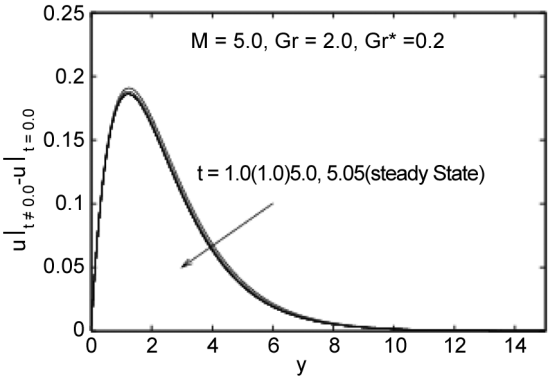

Fig. 20 — Evolution of the horizontal velocity profiles at a time gap of 100 iterations or 1.0 step, $\beta = 0.1$.

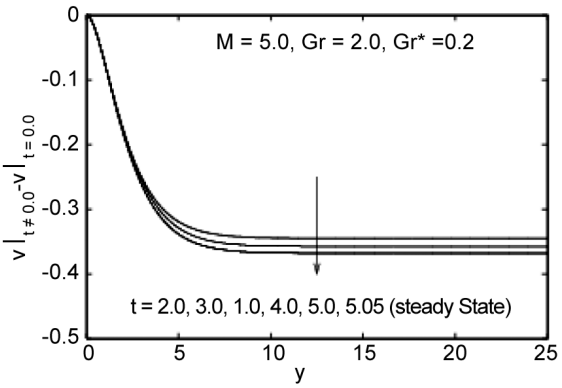

Fig. 21 — Evolution of the vertical velocity profiles at a time gap of 100 iterations or 1.0 step, $\beta = 0.1$.

The local skin friction is observed from Fig. 10, shows a decrease and becomes non-linear with non zero Grashof number near, $(x \to 0)$, then the curves straighten up as $(x \to 1)$. The curve (slope) gets steep (in the negative direction) as the Grash of number increases.

Observing concerning Fig. 4, the steady temperature in Fig. 9, shows a trend reversal compared to the profiles due to applied transverse magnetic field. As a consequence observing Fig. 11, the local Nusselt number shows an increase with the increase in natural convection. Since the local Nusselt number represents the temperature gradient concerning the vertical axis, it shows that the natural convection helps in the transfer of temperature across the vertical direction, hence, an increase in the

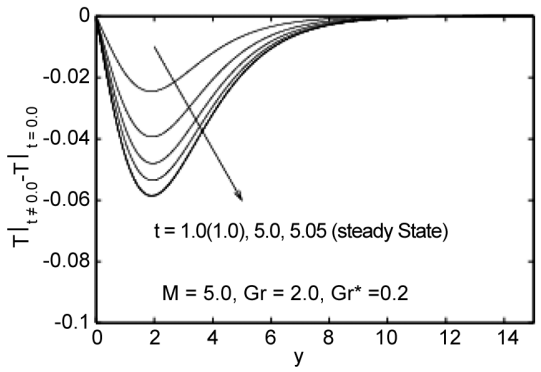

Fig. 22 — Evolution of the temperature profiles at a time gap of 100 iterations or 1.0 step, $\beta = 0.1$.

gradient. The negative sign signifying that this decreases as one moves upwards or y' increases.

Fig. 7-8, shows the velocity profiles for natural convection. The horizontal velocity profiles, Fig. 7, show an increase close to the wall that is $y'/y \to 0$, then drops down after reaching the peak. This shows that the heat transfer is significant near the stretching sheet. The vertical velocity profiles work to compensate for this effect. As expected from Fig. 10, the local skin friction shows a decrease with an increase in natural convection.

From Fig. 12-16, the profiles are described for non-zero Grashof number, *Gr* and Quadratic free convection parameter, *Gr**. The values taken are *M = 0.0, Gr = 0.0, 2.0, 5.0, 10.0*, and the $Gr^* = Gr/10 = 0.0, 0.2, 0.5, 1.0$. Note that the profiles are similar compared to Fig. 7-11. The difference between this set of figures is that they are under the effect of non-zero effect of Quadratic free convection parameter, *Gr**. One can observe from the graphs of Fig. 12, the effect of Grashof number, *Gr*, when it takes increasing values. As the natural convection effect increases the horizontal velocity starts to show a increase. Contrary behavior is observed concerning vertical velocity. The difference can be seen compared to Fig. 2. The effect of natural convection can be used to counter the applied transverse magnetic field. With an increase in the natural convection, the temperature field decreases as seen from Fig. 9. Also, looking at Fig. 10, the local skin friction decreases with the increase in the natural convection. The local skin friction patterns show non-linear behavior as the Grashof number, *Gr*, takes values from 0.0 to 10.0.

The local skin friction shows a decline in the values with an increase in the Grashof parameter, and the Nusselt number shows an increase in the profiles when the Grash of parameter increases as shown in Fig. 11. The curves in this figure show a non-linear behavior with an increase in the Grashof number, *Gr*. This trend can be seen for $y' \to 0$.

In order, to get an insight into the behavior of these curves, Fig. 17-19, shows the difference between the steady-state profiles of velocities and temperature. The curves represented in these figures show the difference between the values of steady-state curves at *Gr** not equal to 0.0 and *Gr** equal to zero. One can conclude that the Quadratic free convection helps in further enhancement of velocities. With an increase in the values of *Gr* and *Gr** one sees that the velocity increase and the scale at which it increases, from these figures. From Fig. 19, the temperature profile also increases in a similar order of magnitude as velocity for an increase in *Gr*,* but in opposite direction. There are only three sets of curves in each of these figures because for the fourth one no difference is observed (*Gr=Gr*=0.0*).

Fig. 20-22, show the time evolution of the patterns of the velocities and temperature profiles. They describe the flow behavior as time progresses.

The evolution pattern does decrease in the case of horizontal velocity and they are of order $\sim 10^{-1}$. However, the temperature evolutionary patterns are distinctly visible. This trend is obvious since the application of natural convection and quadratic free convection subdues the temperature field. Since this being an evolutionary pattern it decreases and gets down to a steady profile.

5 Conclusion

In the present paper, the effect of Quadratic free convection parameter and natural convection along with applied magnetic field effects on the Casson fluid flow moving over a stretching sheet is carried out. The patterns using numerical methods are extracted and analyzed. The major finds include the effect of Quadratic free convection. They act in the backward and aid in further natural convection. The Quadratic free convection effects are seen from the profiles. The findings give a better prospect on the application of Quadratic free convection. The natural convection and the Quadratic free convection effects are counteractive to the applied transverse magnetic field, the Quadratic free convection can be used to bring in mild changes to the actions caused by the applied magnetic field. This can greatly enhance or

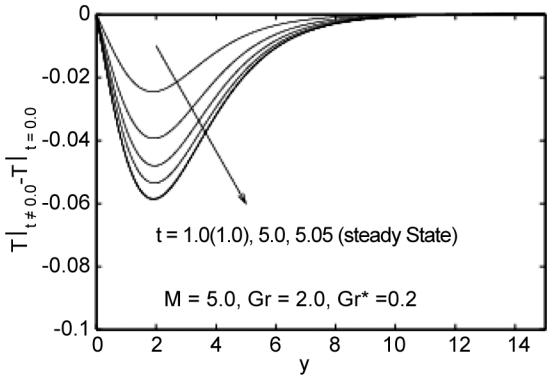

Fig. 22 — Evolution of the temperature profiles at a time gap of 100 iterations or 1.0 step, $\beta = 0.1$.

fine-tune the final product in the manufacturing sector such as Glass and Plastic industry. The investigators believe that the finer aspect of Quadratic free convection can be studied in the future, with other conventional physical aspects of fluid flow. The authors also believe that the present numerical scheme in the form of implicit finite difference method of Crank-Nicolson method can give a very good insight into the flow patterns, considering the inclusion of unsteadiness along with study/investigation/research of steady case fluid flow. Hence, the authors wish to utilize this aspect in further research in this field.

Acknowledgement

The first author wishes to acknowledge the partial financial assistance through TEQIP-III, NIT, Arunachal Pradesh.

The authors would like to thank Prof. (Dr.) P. Pinakeswar Mahanta, Director, National Institute of Technology, Arunachal Pradesh for his persistent encouragement in carrying out this investigation.

The Corresponding author thanks the editor and anonymous reviewer(s) for necessary suggestions and corrections.

The Corresponding author thanks Dr. Ram Prakash Sharma, Associate Professor, Department of Mechanical Engineering, National Institute of Technology, Arunachal Pradesh for the suggestion(s) for improving the presentation of the article.

Nomenclature

List of Symbols

t' Time
x' Horizontal axis
y' Vertical axis
u' Horizontal velocity
v' Vertical velocity
T' Transient temperature
T'_w Wall temperature
T'_∞ Ambient fluid temperature
g Gravitational acceleration
B_0 Transverse magnetic field
$E_{ij}\ (i,j)-th$ component of the deformation rate
C_p Specific heat at constant pressure
Nu_X Local Nusselt number
P_y Yield stress of the fluid
t Dimensionless time
x Dimensionless horizontal axis
y Dimensionless vertical axis
u Dimensionless horizontal velocity
v Dimensionless vertical velocity
T Dimensionless transient temperature
M Dimensionless applied magnetic field parameter
Pr Prandtl number
Gr Grashof number
Gr^* Quadratic free convection parameter
β Heat transfer coefficient
β^* Non-linear volumetric thermal expansion coefficient
Π Product of the component of deformation rate with itself
Π_c Critical value of this product based on the non-Newtonian model
κ Thermal conductivity of fluids
ρ Density of the fluid
σ Electrical conductivity of the fluid
υ Kinematic viscosity of the fluid
τ_{ij} Rheological equation of state
τ_X Local skin friction

References

1 Crane L, *Z Angew Math Phys*, 21 (1970) 645.
2 Gupta P S & Gupta A S, *Can J Chem Eng*, 55 (1977) 744.
3 Kumaran V, Banerjee A K, Kumar A V & Vajravelu K, *Appl Math Comput*, 210 (2009) 26.
4 Ganesan P & Palani G, *Int J Heat Mass Trans*, 47 (2004) 4449.
5 Ramachandra P V, Bhaskar R N & Muthucumaraswamy R, *Int J Therm Sci*, 46 (2007) 1251.
6 Muthucumaraswamy R & Ganesan P, *Comp Meth Appl Mech Eng*, 187 (2000) 79.
7 Arifuzzaman S M, Biswas M U M, Al-Mamun A, Ahmmed

S F & Khan M S, *J Nanofluids*, 7 (2018) 1122.
8 Mondal R K, R E Rabbi, Gharami P P, Ahmmed S F & Arifuzzaman S M, *Math Model Eng Prob*, 6 (2019) 625.
9 R E Rabbi, Arifuzzaman S M, Sarkar T, Khan M S & Ahmmed S F, *J King Saud Univ – Sci*, 32 (2020) 690.
10 Bég O A, Gaffar S A, Prasad V R & Uddin M J, *Int J Eng Sci Tech*, 19 (2016) 377.
11 Ramesh K & Devakar M, *Ain Shams Eng J*, 6 (2015) 967.
12 Kataria H R & Patel H R, *Alexandria Eng J*, 55 (2016) 2125.
13 Khan A, Khan I, Khalid A & Shafie S, *Res Phys*, 7 (2017) 3301.
14 Ahmed S E, Mansour M A, Mahdy A & Mohamed S S, *Int J Eng Sci Tech*, 20 (2017) 1553.
15 Khan A K, Butt A R & Raza N, *Res Phys*, 8 (2018) 610.
16 Mahanthesh B & Gireesha B J, *Res Phys*, 8 (2018) 537.
17 Patel H R, *Heliyon*, 5 (2019) 1.
18 Raza J, *Propul Power Res*, 8 (2019) 138.
19 Buongiorno J, *J Heat Trans*, 128 (2006) 240.
20 Prasad D V K, Chaitanya G S K & Raju R S, *Res Eng*, 3 (2019) 100019.
21 Nandeppanavar M M, Vaishali S, Kemparaju M C & Raveendra N, *Case Studies Therm Eng*, 21 (2020) 100717.
22 Abdelmalek Z, Mahanthesh B, Basir M F M, Imtiaaz M, Mackolil J, Khan N S, Nabwey H A & Tlili I, *Alexandria Eng J*, 59 (2020) 3991.
23 Kumaran V, Kumar A V & Pop I, *Commun Nonlinear Sci Num Simulat*, 15 (2011) 300.
24 Kumaran V, Banerjee A K, Kumar A V & Pop I, *Int Commun Heat Mass Trans*, 38 (2011) 335.
25 Kumaran V, Kumar A V & Pop I, *Acta Mech*, 216 (2011) 139.
26 Kumar A V & Kaliyappan M, *Int J Eng Res Appl*, 3 (2013) 1503.
27 Balamurugan R & Kumar A V, *Int J Mech Prod Eng Res Develop*, 10 (2020) 13355.
28 Balamurugan R & Kumar A V, *Int J Mech Prod Eng Res Develop*, 10 (2020) 13801.
29 Muthucumaraswamy R & Ganesan P, *Nuclear Eng Des*, 215 (2002) 243.
30 Tannehil J C, Anderson D A & Phetcher R H, *Computational Fluid Mechanics and Heat Transfer*, 2nd Edn, Taylor & Francis, (1997).
31 Kumar S M, Sandeep N, Kumar R B & Saleem S, *Alexandria Eng J*, 57 (2018) 2027.
32 Selvaraj A, Dilip J S, Muthucumaraswamy R & Karthikeyan S, *Mater Today*, 46 (2021) 3546.
33 Reza-E-Rabbi S, Arifuzzaman S M, Sarkar T, Khan M S & Ahmmed S F, *J Kind Saud – Sci*, 32 (2020) 690.
34 Krishna M V, Ahamad N A & Chamkha A J, *Ain Shams Eng J*, 12 (2021) 2099.
35 Kumar M A, Reddy Y D, Goud B S & Rao V S, *Int J Thermofluids*, 9 (2021) 100061.
36 Narahari M, Raju S S K & Pendyala R, *Chem Eng Sci*, 167 (2017) 229.
37 Umamaheswar M, Raju M C, Varma S V K & Gireeshkumar J, *Alexandria Eng J*, 55 (2016) 2005.
38 Ramachandra P V, Vasu B & Anwar B O, *Chem Eng J*, 173 (2011) 598.
39 Syafiqah N & Narahari M, *IOP Conf Series: Mater Sci Eng*, 736 (2020) 032020.
40 Narahari M, Ilyas S U & Pendyala R, *AIP Conf Proceed*, 2138 (2019) 030027.
41 Astuti H & Kaprawi S, *Front Heat Mass Trans*, 13 (2019) 1.